A&A 538, A130 (2012)
DOI: 10.1051/0004-6361/201118184

Astronomy & Astrophysics

New observations of chromospheric and prominence activity on the RS CVn-type binary SZ Piscium *(Research Note)*

Dong-tao Cao[1,2,3] and Sheng-hong Gu[1,2]

[1] National Astronomical Observatories/Yunnan Observatory, Chinese Academy of Sciences, Kunming 650011, PR China
e-mail: dtcao@ynao.ac.cn
[2] Key Laboratory for the Structure and Evolution of Celestial Objects, Chinese Academy of Sciences, Kunming 650011, PR China
[3] Graduate University of Chinese Academy of Sciences, Beijing 100049, PR China

Received 30 September 2011 / Accepted 23 December 2011

ABSTRACT

Aims. New high-resolution spectroscopic observations were made for the RS CVn-type binary SZ Psc aimed at searching for evidence of stellar prominences in this system and studying its chromospheric activity.
Methods. By means of the spectral subtraction technique, we searched for prominence-like events in the H_α spectra, and also analyzed several optical chromospheric activity indicators (the He I D_3, Na I D_1, D_2, H_α, and Ca II IRT lines) included in our observations.
Results. The emission in the H_α and Ca II IRT lines show that the cooler component is very active, supporting earlier work. Notably, some absorption features are detected in the subtracted H_α profiles, and one of them may result from prominence-like material on the cooler component of the system. According to a model of stellar prominences, the distance of the prominence from the rotation axis of the cooler component is calculated to be close to the corotation radius and to exceed the Roche lobe of the cooler component.

Key words. binaries: eclipsing – binaries: spectroscopic – stars: activity – stars: coronae – stars: chromospheres

1. Introduction

Stellar prominences have attracted much attention in the past years, and were first reported by Robinson & Collier Cameron (1986) as rapid transient H_α absorption features on the rapidly rotating K0 dwarf AB Dor. These features were interpreted as being caused by prominence condensations of mainly neutral material in enforced corotation with the star by the stellar magnetic field (Collier Cameron & Robinson 1989a). Since then, similar features have been observed on several other rapidly rotating single active stars (Cameron et al. 2002), and also in binary systems (Hall & Ramesy 1992). The observational study of stellar prominence activity not only enriches our knowledge about the magnetic activity, but also has great significance for the study of stellar coronal structure and coronal magnetic field topology.

SZ Psc is an eclipsing double-lined spectroscopic binary consisting of F8V-IV and K1IV components, classified as an RS CVn-type variable star (Hall 1976), with an orbital period of about 3.97 days (Eaton & Henry 2007). It shows strong chromospheric activity, as demonstrated by several optical active lines: Ca II H & K, Mg I b, Na I D_1, D_2, H_α, and Ca II IRT (Jakate et al. 1976; Bopp 1981; Huenemoerder & Ramsey 1984; Fernández-Figueroa et al. 1986; Popper 1988; Doyle et al. 1994; Frasca & Catalano 1994; Fernández-Figueroa et al. 1994; Kang et al 2003; Eaton & Henry 2007; Zhang & Gu 2008).

It is interesting that Zhang & Gu (2008) detected some absorption features in the subtracted H_α profiles of SZ Psc, which may be explained by three possible prominences. In view of this interesting finding, we aim to search for prominence-like events and carried out additional studies for this system in the present work, based on higher time-resolved spectroscopic observations of the H_α line. We derived results on chromospheric and prominence activity of SZ Psc.

2. Observations and data reduction

New high-resolution echelle spectra of SZ Psc were obtained during two observing nights: December 18 and 20, 2010. The observations were carried out with the 2.16 m telescope at the Xinglong station of the National Astronomical Observatories, China. The Coudé echelle spectrograph with a resolving power of about 37 000 and a 2048 × 2048 pixels EEV CCD detector were used during the observations. The spectra have a wavelength range of about 5600–9500 Å, which covers several optical chromospheric activity lines.

The spectrum reduction was performed with the IRAF package, following the standard procedure described by Zhang & Gu (2008). In Table 1, we give the observing log, which includes the observing date, the heliocentric Julian date (HJD), orbital phase, exposure time, and the signal-to-noise ratio (S/N). In order to improve the signal-to-noise ratio for the He I D_3, Na I D_1, D_2, and Ca II IRT spectral regions, several CCD images were combined for these lines, and the resulting spectra were analyzed. The information of those combined images is also included in Table 1. The orbital phases were calculated with the ephemeris HJD = 2 449 284.4483 + 3.96566356 × E (Eaton & Henry 2007).

3. Spectral analysis

We performed the analysis for the normalized spectra of SZ Psc using the spectral subtraction technique described in detail by

Table 1. Observational log of SZ Psc.

Date	HJD	Phase	Exp. time	S/N				
	2 450 000+		(s)	Na I	H_α	λ8498	λ8542	λ8662
2010-12-18	548.9313	0.6810	900	–	87	–	–	–
2010-12-18	548.9420	0.6836	900	–	92	–	–	–
*2010-12-18	548.9420	0.6836	2700	121	–	110	127	121
2010-12-18	548.9527	0.6863	900	–	84	–	–	–
2010-12-18	548.9633	0.6890	900	–	77	–	–	–
2010-12-18	548.9740	0.6917	900	–	75	–	–	–
*2010-12-18	548.9740	0.6917	2700	103	–	91	107	99
2010-12-18	548.9848	0.6944	900	–	72	–	–	–
2010-12-18	548.9954	0.6971	900	–	74	–	–	–
2010-12-18	549.0062	0.6998	900	–	74	–	–	–
*2010-12-18	549.0062	0.6998	2700	99	–	86	101	95
2010-12-18	549.0168	0.7025	900	–	72	–	–	–
2010-12-18	549.0275	0.7052	900	–	72	–	–	–
2010-12-18	549.0491	0.7106	900	–	68	–	–	–
*2010-12-18	549.0517	0.7113	3600	105	–	93	108	101
2010-12-18	549.0598	0.7133	900	–	67	–	–	–
2010-12-18	549.0705	0.7160	900	–	61	–	–	–
2010-12-20	550.9563	0.1915	900	–	84	–	–	–
2010-12-20	550.9672	0.1943	900	–	81	–	–	–
*2010-12-20	550.9672	0.1943	2700	115	–	104	120	113
2010-12-20	550.9780	0.1970	900	–	78	–	–	–
2010-12-20	550.9887	0.1997	900	–	70	–	–	–
2010-12-20	550.9994	0.2024	900	–	66	–	–	–
*2010-12-20	551.0046	0.2037	3600	86	–	84	96	92
2010-12-20	551.0258	0.2091	1800	–	55	–	–	–
2010-12-20	551.0415	0.2130	900	–	56	–	–	–
2010-12-20	551.0522	0.2157	900	–	59	–	–	–
*2010-12-20	551.0540	0.2162	3600	83	–	76	90	87
2010-12-20	551.0684	0.2198	1800	–	66	–	–	–

Notes. (*) Highlight those combined images.

Barden (1985) and Montes et al. (1995). This method has been widely used to estimate the chromospheric contribution in chromospheric activity lines, which subtracts synthesized spectra constructed from reference stars. The validity of the technique applied in searching for prominence-like material in active close binary stars has also been discussed by Gunn & Doyle (1997). For our situation, the synthesized spectra were constructed using the program STARMOD (Barden 1985). We used the two inactive stars HR1536 (F8V) and HD 22072 (K1IV) observed during the same observing run as reference stars.

In the course of the spectral analysis, the first observing night's spectra were used to determine the main parameters. We initially set the $v \sin i$ values to 0 & 78 km s^{-1} (Zhang & Gu 2008) for the two components, and then determined the radial velocity and the intensity weight ratio using the method described in detail by Barden (1985) in the spectra spanning the wavelength region 6381–6789 Å (five echelle orders) except the H_α line. We obtained the radial velocity by averaging the values of the five echelle orders, and adopted the averaging values (0.17/0.83) as the final intensity weight ratio for the H_α spectral region. Secondly, the $v \sin i$ values were recalculated by fixing the values of the radial velocity and the intensity weight ratio. The $v \sin i$ values (3.4 & 76.9 km s^{-1}) of the components of SZ Psc were obtained, which are slightly different from the values published by Zhang & Gu (2008) because different reference stars were used, which have differently intrinsic $v \sin i$ values. Finally, the synthesized H_α spectra were constructed with the parameters calculated above. For the second observing night's spectra, we used the same method to determine the radial velocity by fixing the values of the $v \sin i$ and the intensity weight ratio obtained above, and then constructed the synthesized spectra for the H_α spectral region. For other active lines, the adopted intensity weight ratios are 0.2/0.8 for the He I D_3 and Na I D_1, D_2 spectral region, 0.15/0.85 for the Ca II 8498 spectral region, 0.145/0.855 for the Ca II 8542 spectral region, and 0.14/0.86 for the Ca II 8662 spectral region.

Examples of the observed and synthesized spectra for the H_α line are displayed in Fig. 1, where "H" and "C" represent the hotter and the cooler components. Moreover, using the radial velocities derived above, all subtracted H_α spectra aligned on the cooler component's rest frame are also displayed in Fig. 1.

Table 2. Measurements for the excess emissions of the H_α line.

Phase	EW_{H_α} (Å)	Phase	EW_{H_α} (Å)	Phase	EW_{H_α} (Å)
0.6810	1.451	0.7025	1.638	0.1997	0.962
0.6836	1.472	0.7052	1.694	0.2024	0.964
0.6863	1.588	0.7106	1.678	0.2091	0.891
0.6890	1.508	0.7133	1.648	0.2130	0.833
0.6917	1.541	0.7160	1.627	0.2157	0.786
0.6944	1.598	0.1915	0.877	0.2198	0.889
0.6971	1.604	0.1943	0.959		
0.6998	1.623	0.1970	0.991		

Table 3. Measurements for the excess emissions of the Ca II IRT lines.

Phase	EW (Å)			EW_{8542}/EW_{8498}
	Ca II 8498	Ca II 8542	Ca II 8662	
0.6836	0.677	0.947	0.833	1.399
0.6917	0.614	0.998	0.804	1.625
0.6998	0.622	0.964	0.821	1.550
0.7113	0.634	0.999	0.834	1.576
0.1943	0.442	0.688	0.534	1.557
0.2037	0.465	0.709	0.564	1.525
0.2162	0.483	0.711	0.510	1.472

4. Chromospheric activity

Our observations include several activity indicators: the He I D_3, Na I D_1, D_2, H_α, and Ca II IRT lines, which allow us to simultaneously analyze the behavior of these indictors.

For our situation, the synthesized spectra match the observational ones very well, except for the Na I D_1, D_2 lines, because they are very sensitive to the effective temperature (Montes et al. 1997). Spectral subtraction demonstrates that the H_α and Ca II IRT lines show clear excess emission from the cooler component of the system. We have not found obvious excess emission in the subtracted He I D_3 and Na I D_1, D_2 lines. For the Na I D_1, D_2 lines, Zhang & Gu (2008) detected excess emission from the cooler component at some phases, but no evidence was found in our observations probably because of the different reference stars we used, which may have different effective temperature from those of Zhang & Gu (2008). The measurements for the excess emissions of the H_α and Ca II IRT lines are listed in Tables 2 and 3, respectively, which include orbital phase and the equivalent width, and are plotted against orbital phase in Fig. 2.

The excess emission profiles of the H_α line exhibit broad wings, which obviously extend farther than the wings of the synthesized H_α spectral profiles (see Fig. 1). These broad emission features could be interpreted as arising from microflaring or mass transfer effects, as discussed by Zhang & Gu (2008). Moreover, from Table 3, it can be seen that the EW_{8542}/EW_{8498} values of the Ca II 8542 and 8498 line excess emission are generally low, similar to the results derived by Zhang & Gu (2008), which indicates that the Ca II IRT emissions arise predominantly from plage-like regions.

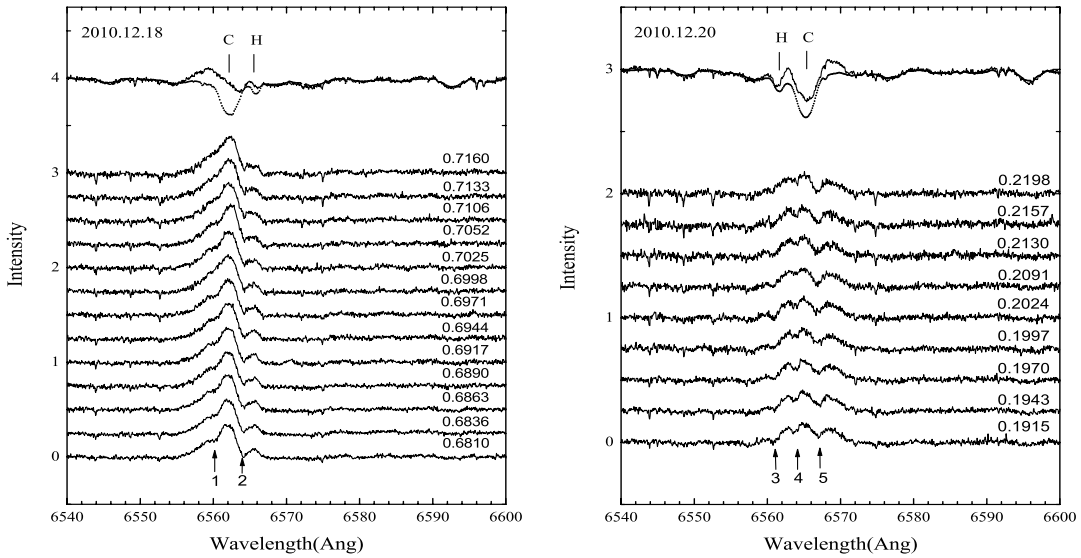

Fig. 1. Observed, synthetic and subtracted spectra for the H_α line. The top lines show an example of the observed (solid) and synthesized (dotted) spectra, while the lower solid lines represent the subtracted spectra. The numbers indicate absorption features appearing in the subtracted H_α spectral profiles.

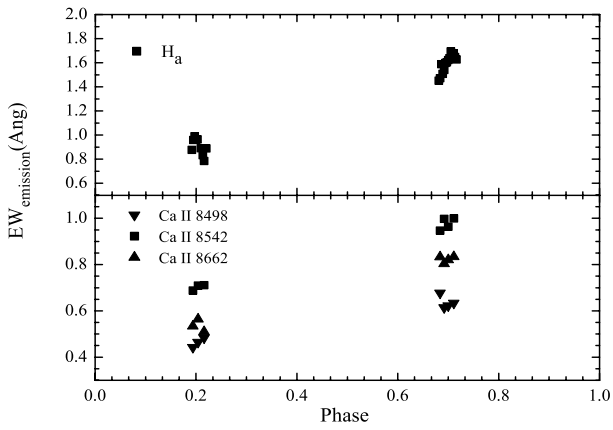

Fig. 2. Equivalent width of the excess emissions plotted against orbital phase for the H_α and Ca II IRT lines.

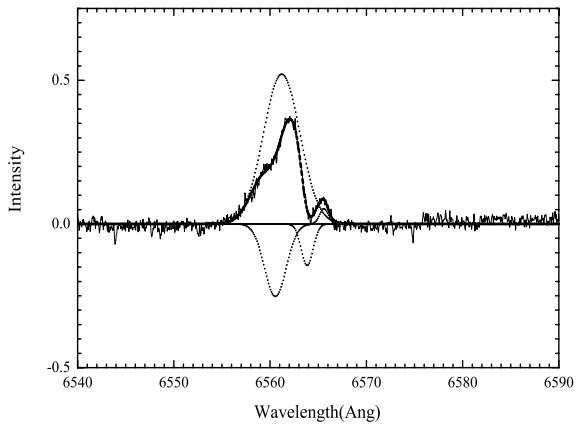

Fig. 3. Example of fitting four Gaussian profiles the H_α residual spectrum, where the solid line indicates the subtracted spectra, and the dotted and dashed lines represent the fitted and summed profiles.

From Tables 2 and 3 and Fig. 2, it can be seen that the level of chromospheric activity for the H_α line and the Ca II IRT lines is higher in the first night (near phase 0.75) than in the second night (near phase 0.25). This indicates possible rotational modulation of the chromospheric activity, which supports the result obtained by Zhang & Gu (2008).

5. Prominence activity

As shown in Fig. 1, several absorption features were detected from the subtracted H_α spectra. They are labeled with numbers for convenient reference in the analysis. The most interesting feature is absorption 1, which appears in the blue wing of the profile and continues to move relative to the cooler component's rest frame. Consequently, a stellar prominence may be the most reasonable explanation for absorption 1, which corotates with the cooler component and scatters the chromospheric H_α emission out of the line of sight when projected against the disk.

We assume that these absorption features seen in the subtracted spectra may result from non-chromospheric activity characteristics superimposed on the chromospheric emission profiles of the system. As shown in Fig. 3, consequently, the subtracted profile can be fitted by four Gaussian profiles, two emission profiles and two absorption ones. To separate the absorption features from the whole profile, we subtracted the stronger profile of the above two emission profiles from subtracted H_α spectra, and used the same profile for each spectrum. The results are displayed in Fig. 4, where we left out the spectra at phases 0.6998, 0.7133, and 0.7160, because the chromospheric emission changed rapidly at these phases, and we clearly see the motion of absorption 1.

For the residual spectra displayed in Fig. 4, the radial velocities of absorption 1 relative to the cooler component's rest frame can be measured, and are listed in Table 4. Consequently, the distance of the prominence from the rotation axis of the cooler component is about $1.9 \pm 0.15\ R_*$ (R_* is the radius of the cooler component) calculated using the formula of Collier Cameron & Robinson (1989a). For the cooler component, adopting the values of parameters from Eaton & Henry (2007): $M_* = 1.74\ M_\odot$, $R_* = 6.0\ R_\odot$, $i = 69°$, its Keplerian corotation radius is calculated to be $R_{kc} = 2.0\ R_*$. Evidently, the prominence is formed close to the Keplerian corotation radius of the cooler component. Moreover, the detected prominence lies outside the

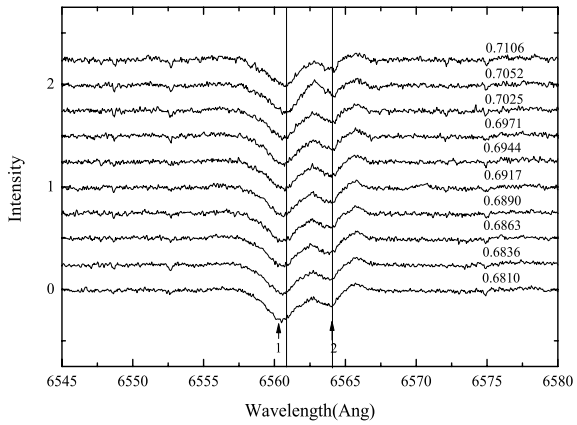

Fig. 4. Results after subtracting a main fitted emission profile from the subtracted H_α spectra. The numbers are the same as Fig. 1, and the vertical lines highlight the motion of absorption features.

Table 4. Radial velocities of absorption 1 relative to the cooler component's rest frame.

Phase	RV (km s^{-1})	Phase	RV (km s^{-1})
0.6810	–80.8 ± 2.0	0.6944	–68.9 ± 1.3
0.6836	–77.5 ± 0.7	0.6971	–67.4 ± 1.2
0.6863	–76.7 ± 2.2	0.7025	–61.9 ± 3.9
0.6890	–75.4 ± 2.4	0.7052	–56.2 ± 1.5
0.6917	–72.9 ± 1.2	0.7106	–54.4 ± 2.8

Roche lobe of the cooler component, which has a radius of about 1.2 R_* (Lanza et al. 2001), this implies it is magnetically confined.

The prominence distance from the stellar rotation axis has been found to lie at or beyond the corotation radius on AB Dor (Collier Cameron & Robinson 1989a,b). For SZ Psc, three possible prominences detected by Zhang & Gu (2008) have projected heights from 2.5 to 3.8 R_*, which are outside the corotation radius, similar to the situation of AB Dor. However, their spectra are not sufficiently time-resolved to trace the prominence's motion, especially for prominence 1 and 2. Fortunately, we tracked the motion of a prominence on this system and derived the projected height from the cooler component, based on higher time-resolved spectra. This is a significant improvement of the results of Zhang & Gu (2008).

Time-resolved observational evidence of stellar prominences in binaries is still scarce, although some excess absorption or emission features in subtracted spectra may be caused by prominence-like material, which had been detected in some RS CVn binaries (Hall & Ramesy 1992). Furthermore, an evolution timescale of a few days for prominence events around single active stars has been reported by several authors (Collier Cameron & Robinson 1989b; Jeffries 1993; Dunstone et al. 2006, etc.). However, it is uncertain whether a similar evolution timescale exists in binaries because of a lack of sufficiently time-resolved observations. Unfortunately, our observations do not allow the lifetime to be estimated. To understand prominence-like events better and estimate their lifetimes on SZ Psc, it is essential that more observations are made for a longer period.

In addition, some other absorption features in the subtracted H_α profiles were also seen. These absorption features are likely not caused by the stellar prominences, because their velocities are not consistent with corotating prominence material. Considering the strong magnetic activity of the cooler component and the extent of its environment, it is reasonable to assume that circumstellar material exists and obscures some parts of the cooler component. Similar phenomena have also been found on the RS CVn-type system AR Mon by Hall & Ramsey (1992).

6. Conclusions

We summarize our results for SZ Psc based on new spectroscopic observations and analysis as follows.

1. The H_α and Ca II IRT lines show that the cooler component is very active, consistent with the results reported by Zhang & Gu (2008).
2. Several absorption features were detected in the subtracted H_α profiles, and one of them may result from prominence-like material on the cooler component. According to a model of stellar prominences, we calculated the distance of the prominence from the rotation axis of the cooler component and found it to be close to the Keplerian corotation radius and to exceed the Roche lobe of the cooler component.

Acknowledgements. We are grateful to Dr. Montes for providing a copy of the STARMOD program. We thank the observing assistants of the 2.16 m telescope of Xinglong station of the National Astronomical Observatories for their support during our observations. We also thank the anonymous referee for his (her) suggestions and comments, which improved the language and clarity of the paper. This work is supported by NSFC under grants Nos. 10373023 and 10773027.

References

Barden, S. C. 1985, ApJ, 295, 162
Bopp, B. W. 1981, AJ, 86, 771
Collier Cameron, A., & Robinson, R. D. 1989a, MNRAS, 236, 57
Collier Cameron, A., & Robinson, R. D. 1989b, MNRAS, 238, 657
Collier Cameron, A., Jardine, M., & Donati, J.-F. 2002, in Stellar Coronal in the Chandra and XMM-Newton Era, ed. F. Favata, & J. J. Drake, ASP Conf. Ser., 277, 397
Doyle, J. G., Mitrou, C. K., Mathioudakis, M., et al. 1994, A&A, 291, 135
Dunstone, N. J., Barnes, J. R., Collier Cameron, A., & Jardine, M. 2006, MNRAS, 365, 530
Eaton, J. A., & Henry, G. W. 2007, PASP, 119, 259
Fernández-Figueroa, M. J., De Castro, E., Montesinos, B., et al. 1986, Adv. Space Res., 6, 187
Fernández-Figueroa, M. J., Montes, D., De Castro, E., & Cornide, M. 1994, ApJS, 90, 433
Frasca, A., & Catalano, S. 1994, A&A, 284, 883
Gunn, A. G., & Doyle, J. G. 1997, A&A, 318, 60
Hall, D. S. 1976, in Multiple Periodic Variable Stars, ed. W. Fitch (Dordrecht: Reidel), 287
Hall, J. C., & Ramsey, L. W. 1992, AJ, 104, 1942
Huenemoerder, D. P., & Ramsey, L. W. 1984, AJ, 89, 549
Jakate, S. M., Bakos, G. A., Fernie, J. D., & Heard, J. F. 1976, AJ, 81, 250
Jeffries, R. D. 1993, MNRAS, 262, 369
Kang, Y. W., Lee, W.-B., Kim, H.-I., & Oh, K.-D. 2003, MNRAS, 344, 1227
Lanza, A., Rodonò, M., Mazzola, L., & Messina, S. 2001, A&A, 376, 1011
Montes, D., Fernández-Figueroa, M. J., De Castro, E., & Cornide, M. 1995, A&A, 294, 165
Montes, D., Fernández-Figueroa, M. J., De Castro, E., & Sanz-Forcada, J. 1997, A&AS, 125, 263
Popper, D. M. 1988, AJ, 96, 1040
Robinson, R. D., & Collier Cameron, A. 1986, Proc. Astron. Soc. Aust., 6, 308
Zhang, L.-Y., & Gu, S.-H. 2008, A&A, 487, 709